Exp Fluids
DOI 10.1007/s00348-007-0267-5

RESEARCH ARTICLE

Microscale 3D flow mapping with μDDPIV

Francisco Pereira · Jian Lu · Emilio Castaño-Graff · Morteza Gharib

Received: 27 March 2006 / Revised: 3 December 2006 / Accepted: 5 January 2007

Abstract Three-dimensional (3D) quantitative flow visualization by tracking microscale particles has become an invaluable tool in microfluid mechanics. Defocusing digital particle image velocimetry (DDPIV) can recover spatial coordinates by calculating the separation between defocused images generated by an aperture mask with a plurality of pinholes. In this paper, a high-speed 3D micro-DDPIV (μDDPIV) system was devised based on this technique to achieve microscale velocity field measurements. A micro-volume of $400 \times 300\ \mu m^2$ with a depth of 150 μm has been mapped using an inverted microscope equipped with a 20× objective lens. The proposed technique was successfully applied to 3D tracking of 2-μm fluorescent particles inside an evaporating water droplet.

Keywords Defocusing · DPIV · 3D · Particle · Tracking · Microfluidics · Microscale · Microscope · Fluorescence · Droplet

F. Pereira
INSEAN—Italian Ship Model Basin,
00128 Rome, Italy

J. Lu
Option of Bioengineering,
California Institute of Technology,
Pasadena, CA 91125, USA

E. Castaño-Graff · M. Gharib (✉)
Graduate Aeronautical Laboratories,
California Institute of Technology,
Pasadena, CA 91125, USA
e-mail: mgharib@caltech.edu

1 Introduction

Quantitative visualization of microscale flow is of great biological and fluid mechanical interest. Particle image velocimetry (PIV) and particle tracking velocimetry (PTV) are essential tools for quantitative flow mapping. Microscale particle image velocimetry (micro-PIV, see Santiago et al. 1998) and microscale particle tracking velocimetry (micro-PTV, see Suzuki et al. 2003) have been developed to measure velocity fields in microscopic fluid flows based on their successful application in macroscale flows. Hove et al. (2003) implemented micro-PIV to measure the velocity and shear stress fields of in vivo cardiovascular blood flow in embryonic Zebrafish.

Micro-PIV/PTV systems have been well applied but are limited to two-dimensional (2D) measurements. However, many microscale fluid flows have 3D characteristics, thus requiring volumetric quantitative imaging techniques to capture the flow 3D features. Holographic PIV (Pu et al. 2000), stereoscopic PIV (Prasad and Adrian 1993) and defocusing DPIV (Pereira et al. 2000), are commonly used in 3D macroscale flow mapping. Recently, many efforts have been directed towards the 3D measurement of microscale flow fields. Following closely the experimental layout used for macroscale stereoscopic PIV, Bown et al. (2005) developed a stereoscopic micro-PIV system based on stereomicroscopy. In this work, a stereomicroscope with two cameras was utilized. The cameras captured particle images from two different angles simultaneously. Vector fields of images from each angle were then obtained by the 2D PIV method. Three-dimensional velocity vectors were calculated by recombining the two vector fields from different

angles. Since microscale flow measurement was achieved with the aid of a microscope, other techniques of microscopy were applied to enable 3D particle imaging. Wu et al. (2005) took advantage of the 3D diffraction ring patterns of small tracer particles when out-of-focus to track 3D particle motions. Defocusing position of a particle was resolved by calculating the radius of the outmost ring. The 3D trajectories of swimming *E. coli* were obtained using this technique.

In the present paper, a microscale 3D flow diagnostic system is described based on the defocusing DPIV technique. The principle of the technique was initially described by Willert and Gharib (1992). Later work by Pereira et al. (2000) and Pereira and Gharib (2002) enhanced the DDPIV concept and introduced an imaging system to map 3D two-phase flow fields. The DDPIV approach is the natural extension of two- and three-component planar DPIV to the full third spatial dimension. Unlike other 3D imaging techniques, such as photogrammetry and holography, the optical arrangement in a DDPIV system has a single optical axis. This conveys a number of unique advantages such as use of out-of-the-shelf components, compactness of the instrument and ease of implementation. DDPIV holds many analogies with a standard 2D imaging system, where the light scattered by a point source is collected through a converging lens and a single aperture, located usually on the lens axis. In contrast, the DDPIV technique uses a mask with a multiplicity of apertures, arranged in a predefined pattern, to obtain multiple images from each scattering source. These images form the same geometrical figure on the image plane, but scaled according to the depth location of the scattering source. Hence, the particle's 3D location can be determined, through simple ray-optics relationships, by measuring the centroid and size of the pattern on the image plane. DDPIV maps instantaneously a given volume of interest and provides sets of particles quantitatively located in the physical space. If such particle sets are recorded in time, it is then possible to reconstruct their time evolution in space in a Lagrangian manner and derive their individual displacement and velocity, following the particle tracking methodologies described in Pereira et al. (2006).

The DDPIV principle is here applied for use with an inverted microscope, with the multiple pinhole aperture implemented into a standard unmodified microscope objective. The concept is not original in essence, since the implementation of a mask with multiple apertures into a single lens for the purpose of fluid diagnostics was first proposed by Willert and Gharib (1992). This concept implicitly extends to all sorts of lenses, including a microscope objective. Recently, Yoon and Kim (2006) applied successfully the Willert and Gharib's (1992) approach to capture the 3D flow field over a backward-facing step in a 50-μm deep micro-channel. However, in each implication, there exist calibration challenges that may pose severe difficulties in obtaining reliable information. The central problem with implementing the defocusing principle in a microscope resides in the complexity of the optical path and in the fact that the optical specifications of the objectives used therein are generally not accessible. Aware of this, Yoon and Kim (2006) describe a calibration-based method where calibration curves are constructed that link the size of the multiple-image pattern to the depth location, hence departing from the geometrical optics analysis typical of traditional DDPIV. Furthermore, their work does not provide the necessary uncertainty analysis that would help characterize a generic microscopic DDPIV system.

Therefore, the present work will address some of these difficulties, which are inherent in the work of Yoon and Kim (2006), and propose a practical solution to resolve the calibration issues. We suggest an alternate approach to the calibration problem that preserves the integrity of the DDPIV framework. An original calibration methodology is laid out where the optical characteristics of the system are derived in order to enable the use of the standard DDPIV analysis, as in a macroscale DDPIV apparatus. Moreover, this allows us to apply the uncertainty analysis introduced by Pereira and Gharib (2002) and further extended by Kajitani and Dabiri (2005). We describe the technique, with a special emphasis on the calibration procedure and measurement uncertainty. To demonstrate the functionality of the proposed micro-DDPIV (μDDPIV) system, and without going into physical considerations, we apply the technique to obtain time-resolved quantitative volumetric information on the internal flow of an evaporating water droplet.

2 Experimental setup

A schematic of the experimental setup is shown in Fig. 1. The optical system consists of a microscope, a three-pinhole aperture mask, an argon-ion laser and a high speed CCD camera. An inverted microscope (Nikon® Eclipse TE2000-S) was utilized to implement the defocusing technique. An aperture mask with three pinholes forming an equilateral triangle was attached to the back of a 20× objective lens (Nikon® Plan Apo, NA = 0.75). The diameter of the pinholes is 2 mm and the separation between each two pinholes is 7 mm. In a

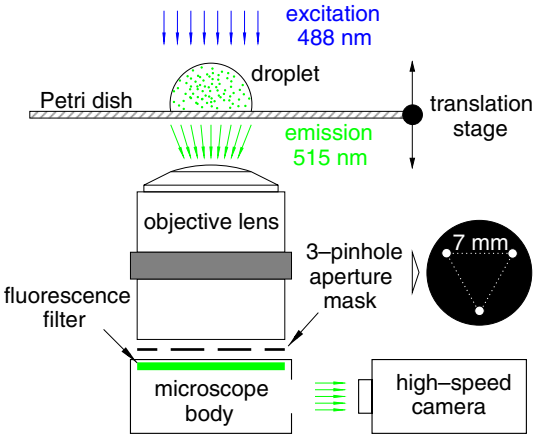

Fig. 1 Schematic of the μDDPIV experimental setup

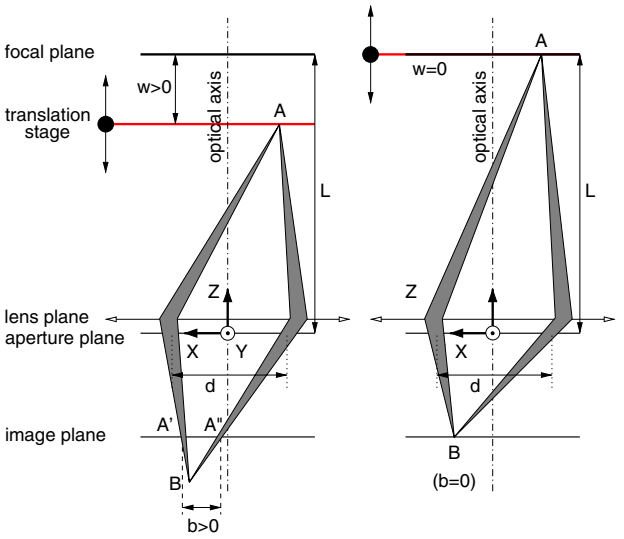

Fig. 2 μDDPIV optical schematic

conventional DDPIV system, only the distance between object space and lens plane is allowed to change. Since any adjustment of the focus of the inverted microscope would have caused a change of the distance between the lens plane and the image plane, the focus knob has been locked during the performance of the measurements. Thus, the built-in horizontal stage on the microscope was replaced by a vertically mounted 1-μm resolution stage to allow adjustment along the axial direction (Z) of the distance to the measurement domain. As regards the illumination, bright field microscopy was initially adopted. However, the droplet air–liquid surface was causing strong reflections, consequently hindering the particle detection because of the poorly contrasted images. Therefore, fluorescence microscopy, which is broadly used for biological imaging and small scale fluid visualization, was chosen to perform the experiments. We chose 2-μm yellow–green fluorescent microspheres (Molecular Probes® FluoSpheres) as the flow markers. We used the 488 nm spectral line of a 5 W argon-ion laser to excite the microspheres, the emission line of which is 515 nm. The illumination of the measurement domain was done through the optical path normally used for regular bright field imaging. Time series of defocused images were recorded using a high speed CCD camera with 512×384 pixel^2 resolution (Kodak® EktaPro Motion Analyzer, Model 1000HRC). The frame rate was 250 frames per second.

3 Calibration

3.1 Principle

Figure 2 shows a schematic of a DDPIV optical configuration, composed of only two apertures for clarity of explanation. Let the coordinates of the system be (X, Y, Z), with the Z-axis corresponding to the optical axis. A point A out of the focal plane focuses on a point B beyond the image plane and, because of the off-axis apertures separated by the distance d, generates two images A' and A'' on the image plane, separated by the distance b. If point A is moved back to the focal plane, the two images coincide on the image plane with $b = 0$.

Pereira and Gharib (2002) used a geometrical analysis to determine the relationship between the (unknown) depth coordinate Z and the separation b between the multiplicity of defocused images of a given particle. This approach requires knowledge of parameters such as the distance L between the focal plane (also referred to as the reference plane) and the aperture plane, the mean separation d between pinholes in the aperture mask and the focal length f of the lens. The latter parameter is also related to the objective magnification M by the lens formula: $f = ML/(1 + M)$.

Unfortunately, for a microscope-based system, the actual optical properties of the objective lens are not generally accessible. In addition, the axial position of the objective optical center, and therefore of the aperture plane, cannot be explicitly measured in absolute terms. For these reasons, the standard DDPIV geometrical analysis, as outlined in the previous works, is not readily applicable for the μDDPIV system proposed here.

However, it is possible to determine the unknown parameters through calibration. Indeed, the separation b is related to the depth coordinate Z by the following relation, see Pereira and Gharib (2002):

$$b = MdL\left(\frac{1}{Z} - \frac{1}{L}\right) \quad \text{with} \quad 0 < Z \leq L \tag{1}$$

M and d are known parameters of the optical system: M is given by the objective prescription and d is a design characteristic of the aperture mounted into the objective. Hence, we shall rewrite Eq. (1) in the following form:

$$L = Z\left(\frac{b}{Md} + 1\right) \tag{2}$$

M and d being known, a measure of b at a known position Z would suffice to determine L, which does not depend on Z nor on any optical parameter. However, as we pointed out before, the absolute position of the lens optical center is not known a priori, thus the Z-origin is also unknown in absolute terms. Let $Z = L–w$, where w is the relative distance of a given point A to the reference plane, see Fig. 2. From Eq. (2) we can then express L as a function of w:

$$L = w\left(\frac{Md}{b} + 1\right) \quad \text{with} \quad w = L - Z, \;\; Z < L \tag{3}$$

Hence, the problem is now reduced to the determination of the actual origin for w. This origin shall define the location of the reference plane. Although L is unknown, the reference plane can be practicably located if one uses a target composed of a transparent plate speckled with marker particles, and translates it by means of a precise translation device (see Fig. 2) along the Z-axis until the b separation is cancelled ($b = 0$). This particular position corresponds also to $w = 0$. Figure 3 shows triple images of particles (or DDPIV images) obtained with our 3-aperture microscopic setup (Fig. 1) for three different values of w. Setting the precision positioning system for any value of w such that $w > 0$, and consequently measuring the separation b, automatically defines L through Eq. (3). Once L is determined, one can calculate the focal length by simply using the lens formula. The optical system is then fully characterized and the standard DDPIV formulas can be applied normally.

We shall stress out that this procedure should be performed from a statistical standpoint, hence a large number of measurements are recommended to obtain statistically representative estimates. This can be done by performing repeated measurements across the observation volume. In addition, the derived parameters L and f do not necessarily match the actual characteristics of the microscope optics. However, they allow reducing the whole microscopic setup to an equivalent single lens system, suitable to apply the DDPIV conceptual approach.

3.2 Experimental procedure

To perform the calibration, we used the 2-μm fluorescent microspheres as the calibration targets. It is known that diffraction and spherical aberration in microscopic imaging may cause distortion of defocused images (Inoué and Spring 1997). Therefore we used a few targets that we spread over a transparent plate to calibrate the defocusing instrument. To manage this micro-target setup, we diluted the fluorescent particles into de-ionized water and put one droplet of diluted solution onto an optically transparent plastic Petri dish (see Fig. 1). After a few minutes, water would evaporate completely and particles would dry-mount on the plate. The mounted particles were then placed under the microscope and defocused by moving the translation stage, see Figs. 1 and 2. The camera captured defocused images of particles located at different distances w away from the focal plane. The Petri disk was moved in one direction starting from the reference plane ($Z = L$, $w = 0$), where the defocused images overlap (separation $b = 0$), up to a point of maximum separation where detection was not possible. The target was moved in steps of 10 μm starting from the reference plane, totalling a depth range of 110 μm.

Figure 4 describes the image processing performed prior to the triangle pattern matching (for details, see Pereira and Gharib 2002). In particular, the high-speed camera uses a CCD sensor split into 16 areas, each 64 × 196 pixels. Each area has a separate gain amplifier, causing the image to show a non-uniform

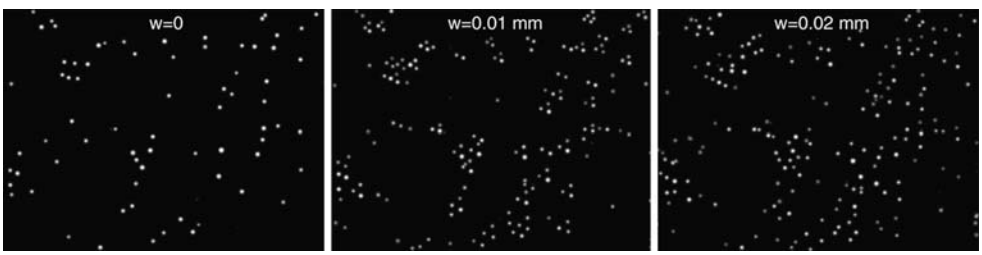

Fig. 3 μDDPIV images as a function of **w**

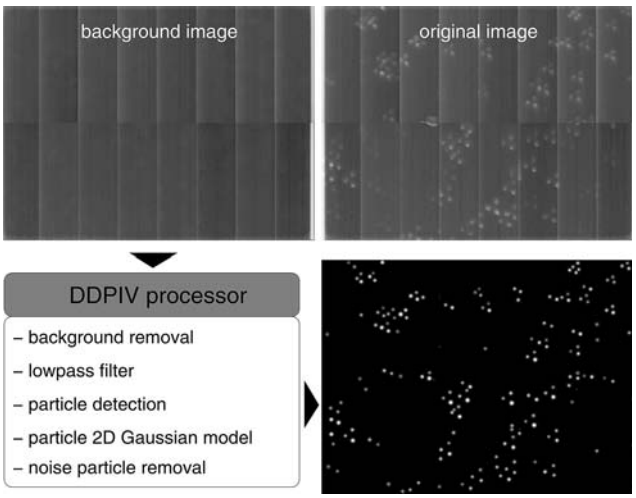

Fig. 4 Image processing (background and original images are enhanced for display)

background. We recorded an image of this background in darkness conditions. The resulting image, shown in Fig. 4, was then subtracted from the particle image. Further processing includes lowpass filtering, particle subpixel detection, particle 2D Gaussian modeling and noise particle removal. This latter operation filters out the particles based on their image size.

3.3 Results

For each position w of the target plate, we measure the image separation b of each particle and calculate its mean value and root mean square error. These two quantities are reported in Fig. 5. Since b is zero for $w = 0$, no (or very limited) information is available at the starting Z position. Sample triangle images are shown to illustrate the increasing pattern size as w is increased. The pattern is reduced to a point when $w = 0$. The depth range of the current μDDPIV system is found to be approximately 110 μm.

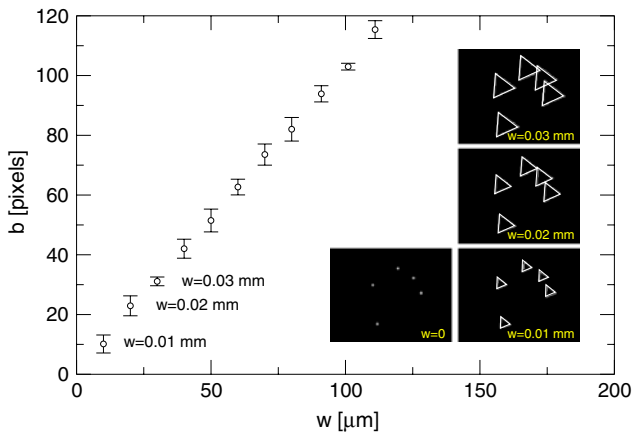

Fig. 5 Mean separation b and RMS as a function of the relative distance w

Figure 6 shows the corresponding focal distance L, on a per-particle basis. One immediately observes that L is not dependent on w, as expected. We obtain for L a mean value of 7.9765 mm with a standard deviation of 393.5 μm. The resulting focal length f is 7.597 mm. The error on the mean value has four main sources. The first is related to the Z-positioning system, which has a limited resolution of 1 μm with an analog reading that affects the final accuracy on the reference displacement w. The second derives from the reduced CCD sensor size of the high-speed camera used in this experiment, source of a limited image resolution (1.166 pixel/μm on the image). The third is linked to the DDPIV processor itself, which introduces errors at the particle peak detection level, even though subpixel algorithms are used. Finally, optical aberrations and geometrical distortions are not fully accounted for. In that latter case, errors can be partly overcome (as suggested by Pereira and Gharib 2002) following the distortion compensation procedure proposed by Soloff et al. (1997). A larger dispersion is observed for small w, where the pattern size is equally small, inducing larger relative error on the measurement of the image separation b.

Using these calibrated parameters and Eq. (1), the images are reprocessed to obtain the absolute depth Z with the following relation:

$$Z = L\left(1 + \frac{b}{Md}\right)^{-1} \tag{4}$$

Figure 7 represents the measured relative displacement, named w_m, versus the actual displacement w of the target. The regression line is also reported. The relative error $|w_m - w|$/FS, where FS stands for full scale and represents the depth range of the current μDDPIV system (110 μm), is within 3%.

The system sensitivity is defined as the separation change for a given Z-variation, and is expressed as

$$\frac{\partial b}{\partial Z} = -\frac{MdL}{Z^2} \quad \text{with} \quad Z = L - w \tag{5}$$

We report in Fig. 8 the evolution of this quantity as a function of the distance w to the focal plane. The b-gradient is found to be fairly constant across the full measurement depth, with a variation of only 4% of FS and an average value of about 1.04 pixels for a displacement of 1 μm along the out-of-plane direction.

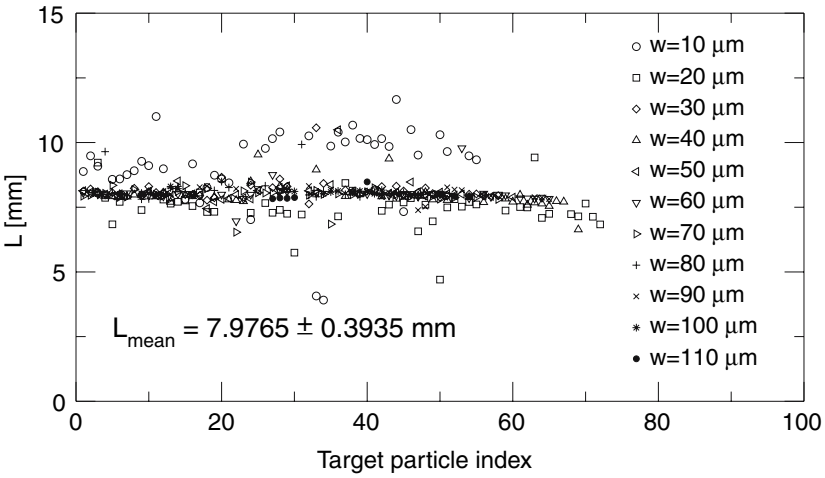

Fig. 6 Focal distance L versus w, and mean estimate

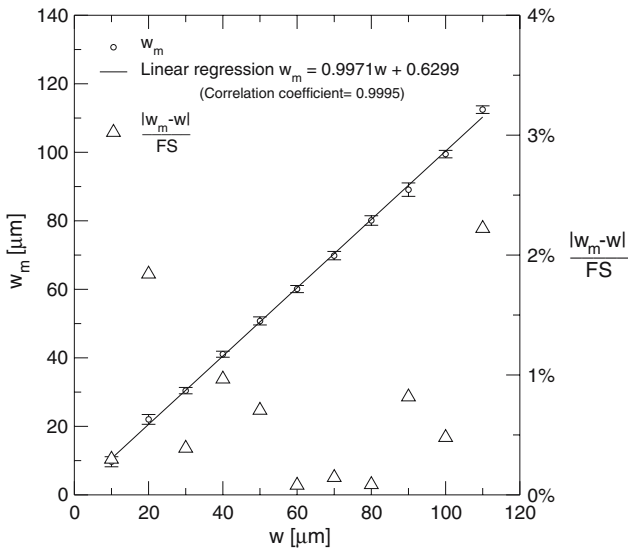

Fig. 7 Measured distance w_m to focal plane versus reference displacement w, and relative error with respect to the total depth range (full scale FS)

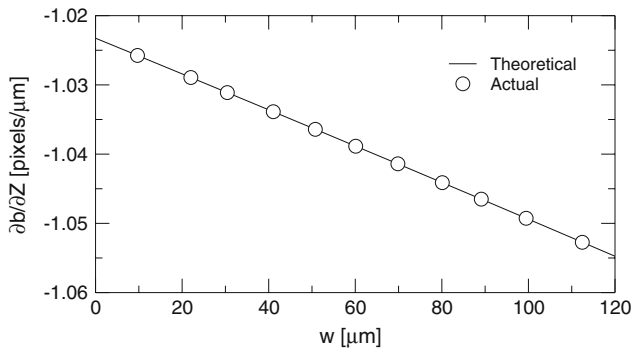

Fig. 8 Sensitivity curve of the current μDDPIV system

The image coordinates of the particle centroid are calculated using the subpixel algorithms described in Pereira and Gharib (2002). The particle images are modeled with non-isotropic 2D Gaussian functions estimated through least squares minimization methods. Pixel resolutions lower than a tenth of a pixel are common with less accurate techniques such as the 3-point Gaussian fit or the bilinear interpolation. Hence, based on the above results, we can reasonably state that the depth resolution of the μDDPIV system assembled here is lower than 100 nm (i.e. <0.1% of FS).

4 Uncertainty analysis

Hereafter, the measurement uncertainties are established and discussed. In this respect, theoretical developments are readily available in the literature: Pereira and Gharib (2002) have laid out the formulas for a generic DDPIV layout with two apertures. Kajitani and Dabiri (2005) have extended these formulas to describe a DDPIV system composed of three apertures arranged in the form of an equilateral triangle. This latter layout has been implemented in most of the macroscale DDPIV systems developed so far (see for instance Jeon et al. 2003) and is also the configuration used for the μDDPIV setup proposed here.

Let $\delta(dX)$, $\delta(dY)$ and $\delta(dZ)$ be the measurement uncertainties on the object space displacements (dX, dY, dZ) along X, Y and Z, respectively. Table 1 summarizes the relationships given by Pereira and Gharib (2002) and by Kajitani and Dabiri (2005), with $K = 1/MdL$. Δx represents the uncertainty on the image plane, i.e. the uncertainty on the determination of the pixel location of a particle image centroid. Note that the uncertainties on X and Y are identical in Kajitani and Dabiri (2005), while they differ in the work by Pereira and Gharib (2002) because of the 2D derivation used therein.

Table 1 Uncertainty definitions, according to Pereira and Gharib (2002) and Kajitani and Dabiri (2005); $K = 1/MdL$

Uncertainty type	Pereira and Gharib (2002)	Kajitani and Dabiri (2005)
$\delta(dX)$	$Kd\lvert Z\rvert\Delta x\sqrt{1+\frac{2X^2}{d^2}}$	$\frac{d}{\sqrt{3}}K\lvert Z\rvert\Delta x\sqrt{1+\frac{3X^2}{d^2}}$
$\delta(dY)$	$\frac{d}{\sqrt{2}}K\lvert Z\rvert\Delta x\sqrt{1+\frac{4Y^2}{d^2}}$	$\frac{d}{\sqrt{3}}K\lvert Z\rvert\Delta x\sqrt{1+\frac{3Y^2}{d^2}}$
$\delta(dZ)$	$\sqrt{2}KZ^2\Delta x$	$KZ^2\Delta x$

To establish the measurement uncertainties $\delta(dX)$, $\delta(dY)$ and $\delta(dZ)$, we consider the trajectories of the individual calibration particles used in the previous section and calculate their deviation in all three directions from the actual path, which is a pure translation along the Z-axis. In a sense, we use the calibration dataset as a flow test case to qualify the performance of the μDDPIV system. We represent in Fig. 9 the experimentally determined uncertainties, expressed in terms of root mean square errors, as a function of the distance w to the focal plane. This figure shows that the uncertainty levels on the particle in-plane location (i.e. X and Y coordinates) are fairly equal, as expected. This is also in full agreement with the theoretical formulations reported in Table 1. The in-plane uncertainty is about 0.5 µm. For the out-of-plane component, the uncertainty is found to be larger with a mean value of 1.2 µm. The in-plane uncertainty has a slightly decreasing trend starting from the focal plane ($w = 0$) that is in agreement with the linear relationship existing between $\delta(dX)$ and $\delta(dY)$ and the depth coordinate Z, for constant X and Y respectively. Beyond $w = 50$ µm, the trend has a seemingly increasing behavior, which could possibly be an effect of the image blurring that takes place as the particles move away from the focal plane, hence affecting their intensity and their detection, and ultimately the particle location error. A parametric study based on particle size and aperture characteristics would be desirable to identify the elementary sources of errors and to better quantify their individual contribution to the overall performance.

The ratio between the out-of-plane and the in-plane uncertainties is a useful parameter that is generally considered to measure the overall performance of a three-component measurement system, as outlined in Prasad and Adrian (1993) and Pereira and Gharib (2002). For a three-aperture system, Kajitani and Dabiri (2005) give the following expression for the ratios ε_X and ε_Y of the out-of-plane error $\delta(dZ)$ to the in-plane components $\delta(dX)$ and $\delta(dY)$, respectively:

$$\varepsilon_\Phi = \frac{\delta(dZ)}{\delta(d\Phi)} = \frac{\sqrt{3}|Z|}{d\sqrt{1+\frac{3\Phi^2}{d^2}}} \quad \text{with} \quad \Phi \equiv X, Y \tag{6}$$

We report in Fig. 10 the values of these ratios, versus the distance w to the focal plane. We also plot the theoretical value, as per Eq. (6), calculated at the centerline of the optical system ($X = Y = 0$) where ε_X and ε_Y reach their maximum. The measured ratios are found to be slightly larger than the theoretical value, with a mean of 2.4 µm for ε_X and 2.33 µm for ε_Y, while the predicted value is sensibly constant at 1.96 µm. However, there is an overall strong agreement between the actual and the theoretical trends that confirms the well-sounded nature of the calibration approach.

It is important to underline the fact that the out-of-plane error is only two to three times larger than the in-plane components. This is a peculiar characteristic of the μDDPIV layout implemented here (and of any μDDPIV system in general) and is a consequence of the fact that the focal distance is nearly equal to the aperture separation d. This result is in strong contrast

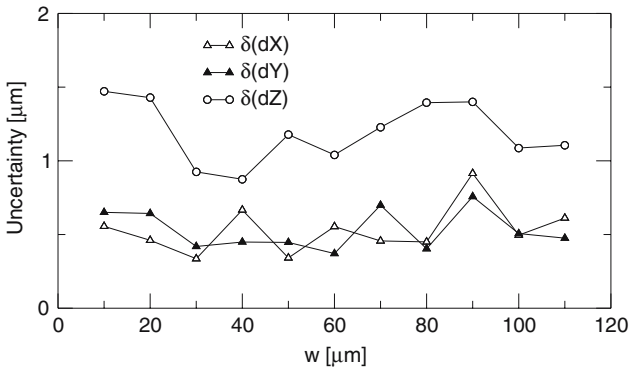

Fig. 9 Uncertainty levels on the space displacements dX, dY and dZ

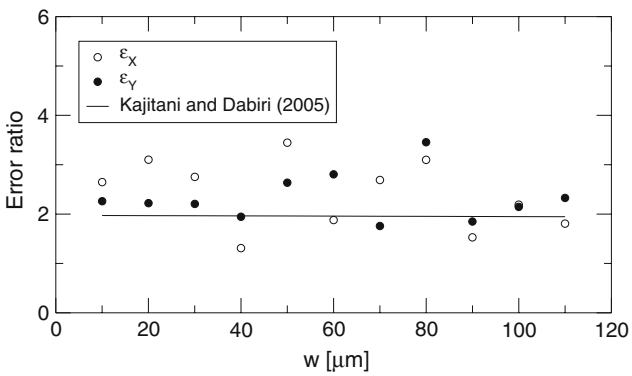

Fig. 10 Out-of-plane to in-plane error ratios ε_X and ε_Y

with that generally found with a macroscopic-type DDPIV design, where the focal distance L is typically much larger than the aperture separation d. Pereira and Gharib (2002) report ratios varying from 4 to 6 for an error-free system with $L = 1{,}000$ mm and $d = 100$ mm. Hence, higher magnification objectives (i.e. >20×) are expected to provide even better performance, at the cost of shallower mappable volumes.

Finally, we estimate the image uncertainty Δx, expressed in pixel units, from the equations listed in Table 1 and we report the result on Fig. 11. As expected, Δx is found to be fairly constant across the volume depth, with a mean value of 1.077 pixels and a standard deviation of 0.145 pixels.

5 Application to the internal flow of an evaporating water droplet

In order to demonstrate the functionality of our micron-scale DDPIV system, the 3D internal circulation of a small evaporating droplet on a solid surface was quantified using the particle tracking approach (see Pereira et al. 2006).

Very little work has been done in the past to obtain quantitative information on the flow inside an evaporating droplet. To our knowledge, the work by Kang et al. (2004) is so far the only available source providing such experimental information. Kang et al. (2004) have devised a mapping method based on ray tracing to correct for the strong image distortion caused by the refraction of light at the air–water interface of the droplet. Illuminating the droplet with a thin laser light sheet and observing the flow with a long-distance zoom lens, they applied the PIV technique and their correction method to obtain planar two-component velocity fields. They could in particular demonstrate the existence of a vortex-type convection flow during the evaporation process. However, 3D flow mapping is a necessity if one wants to address issues related to the droplet evaporation mechanism, such as the effect of Marangoni instabilities or the effect of the contact angle, as well as the evaporation rate. We present here sample volumetric three-component velocity fields of such a flow.

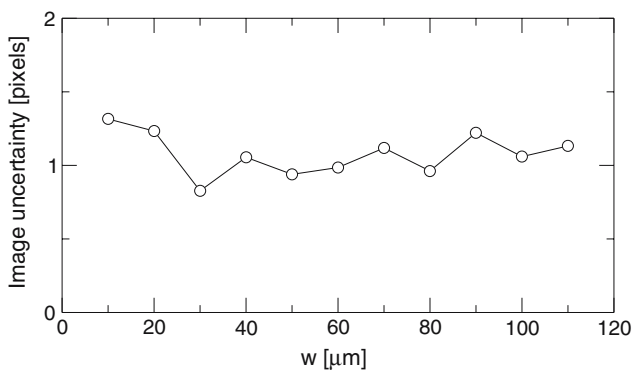

Fig. 11 Uncertainty on the pixel coordinates

A solution with 5% ethanol in de-ionized water was used as the evaporating liquid in this experiment. The 2-µm yellow–green fluorescent microspheres were added to the solution as tracer particles. A droplet of 2 µl was placed on a Petri dish with a micro-pipette. The diameter of the droplet was about 2 mm. Flow image sequences of the internal circulation were captured and recorded by the high-speed camera at 250 frames per second. Note that the use of an inverted microscope eliminates the image distortion and light scattering problems reported in Kang et al. (2004).

We present two cases, performed under different experimental conditions. The purpose is primarily to illustrate the use and potential of μDDPIV. Further work is ongoing on the physical aspects of the flow, however those are not contemplated nor discussed in the present work.

5.1 Particle tracking

The PTV method tracks individual particle images in consecutive image frames and computes the directionally resolved vector for each matched particle. Among the many tracking algorithms available, the relaxation method has been chosen, following the work by Pereira et al. (2006) who implemented the scheme into DDPIV and thoroughly assessed its performance against other state-of-the-art tracking methods. This algorithm has been proved to be superior, both in performance and robustness, to these other approaches. The basic concept of particle tracking in the relaxation method is to search for the most probable link of a given particle while assuming similar displacements of its neighbor particles (the so-called quasi-rigidity condition), within a neighborhood of specified size. Thus, the search for the matching particle in the next time step is made in the direction that the neighbor particles are most likely pointing to. In an iterative process, the probability of the link is gradually increased towards unity while the other probabilities tend to zero. After successful termination of this iterative process, which is applied to every particle, the correct particle links are those with the highest probabilities.

5.2 Case 1

Figure 12 shows, on the top image, the accumulated information of the 550 DDPIV images recorded in the

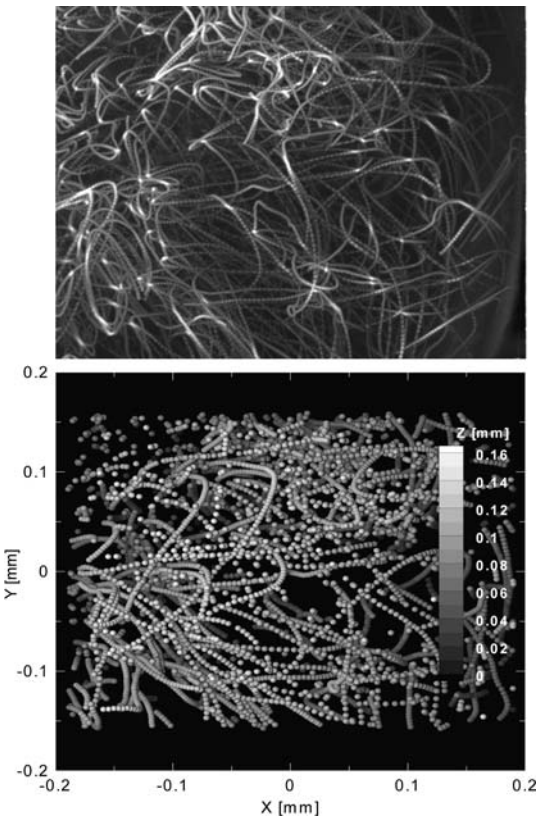

Fig. 12 Droplet internal flow (*case 1*): sequence of 550 DDPIV triple-aperture images (*top*) and corresponding reconstructed particle field (*bottom*)

first sequence, and shows the complex trajectories of the fluorescent markers as they are transported by the internal flow. Note that, on any single image obtained with the μDDPIV design employed here, every flow marker is represented by a triplet of particle images (see Fig. 3 for an example). Hence the image shown in Fig. 12 only provides a view suggestive of the actual flow as seen through the lens of the μDDPIV system. The bottom plot represents the corresponding reconstructed particle field, where the particles are individually located in space and time. The domain has been translated to the microscope system's origin, hence $Z = 0$ represents the surface of the Petri dish on which the droplet has been deposited. The volume depth is slightly less than 160 μm, while the field of view is about 400×300 μm^2. The particles moving beyond the focal plane ($Z > L$) are also imaged and produce an inverted pattern on the image plane. We have processed these situations equally, thus explaining the extended range of measurement (160 μm) with respect to the calibration results (110 μm).

5.3 Case 2

In this second case, the droplet was seeded with the fluorescent particles at a lower density. Figure 13 shows the reconstructed particle field together with the

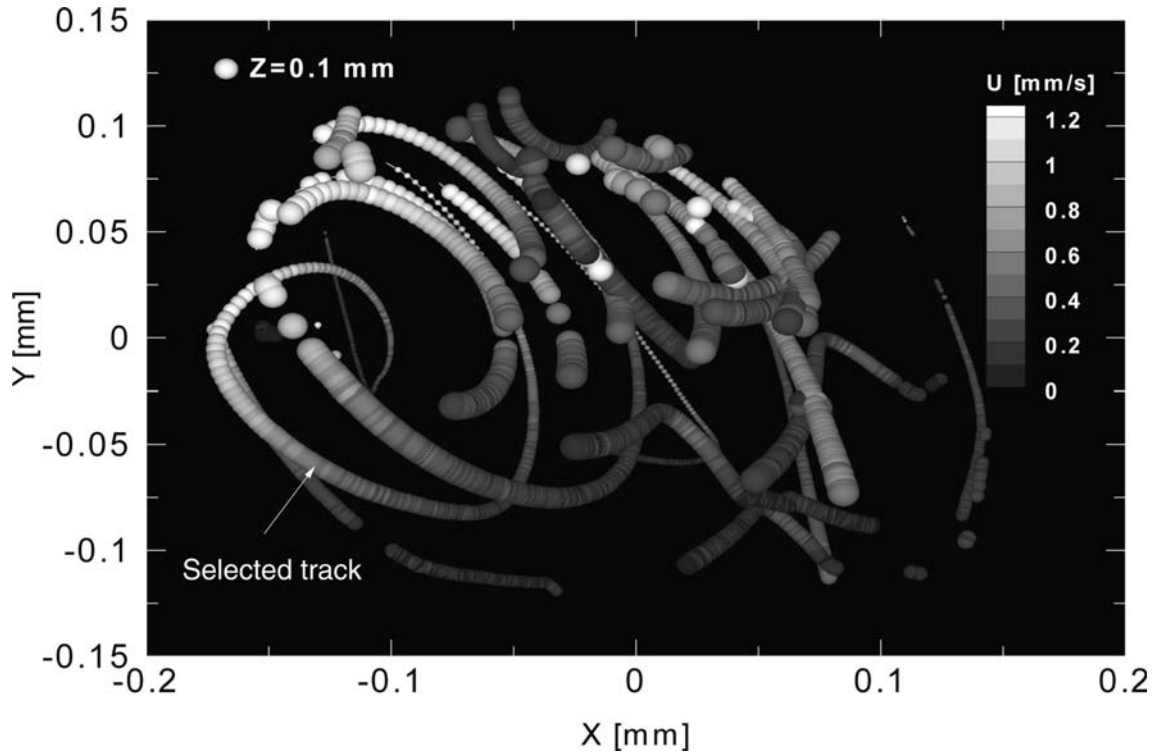

Fig. 13 Droplet internal flow (*case 2*): particle and velocity fields; size of markers is proportional to Z

velocity field, calculated using the tracking technique. The size of the particle markers on the plot is proportional to their Z-location within the droplet, while their gray level is indicative of their velocity. As in the previous case, the volume is shown translated to the system's origin, with $Z = 0$ indicating the Petri dish surface. The volume depth is 100 μm and the field of view is about 300×250 μm^2. The maximum velocity is approximately 1.3 mm/s.

To further illustrate the potential for Lagrangian analysis of the method proposed here, we isolated a particle (see Fig. 13) and reconstructed its path in space and time. We developed a long-time tracking algorithm to establish the particle link from frame to frame. Hence, by selecting a particle in a given frame, the algorithm reconstructs its complete path by tracking the particle in the neighboring frames in a backward and forward process. Figure 14 represents one such single particle track, extracted from the data shown in Fig. 13. We also report the projection of the track on the planes XY, XZ and YZ to help visualize the 3D trajectory. Figure 15 shows the evolution of the velocity vector (U_x, U_y, U_z) and of the acceleration (U_x', U_y', U_z') of this single particle as a function of time. Minute information on the particle motion is shown in Fig. 16, which represents the fluctuations along the X-axis of the particle position with respect to its mean path. The plot shows a periodic motion of the particle, which is also observed on the other axes (not shown here). The frequency of the fluctuation is about 100 Hz and the standard deviation is 200 nm, as clearly visible in the inset plot. This motion has no physical origin and is believed to be an artifact of the experimental setup, most probably a structural vibration induced by a rotating mechanical part. However, it allows us to clearly illustrate the capability of the μDDPIV technique, as implemented here, to capture and isolate a submicron scale feature of the flow. It also confirms the 100-nm resolution performance estimated during the calibration process.

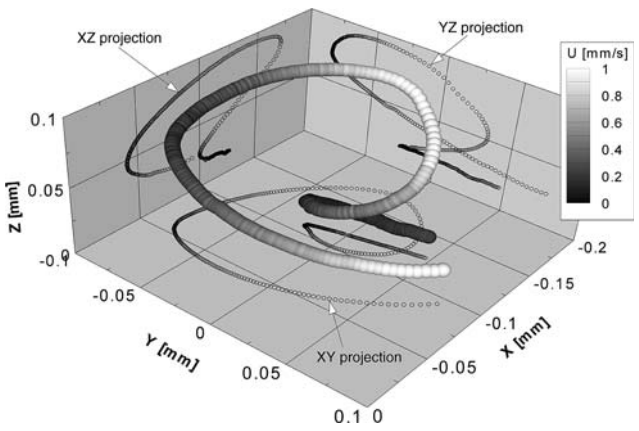

Fig. 14 Droplet internal flow (*case 2*): velocity magnitude along the selected track

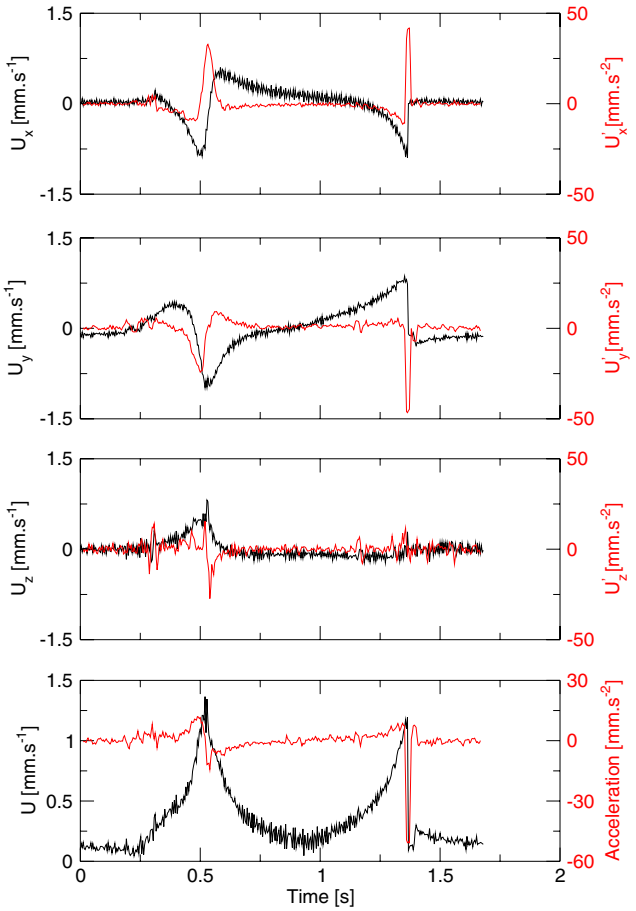

Fig. 15 Velocity (*black*) and acceleration (*red*) history along the extracted track

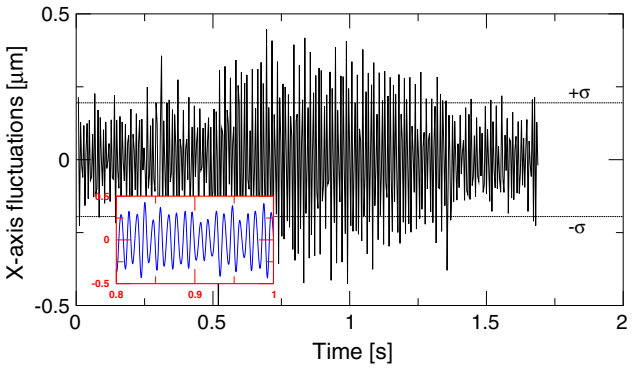

Fig. 16 Particle X-fluctuations along the extracted track

6 Conclusion and perspectives

A 3D visualization system was devised based on the defocusing DPIV (DDPIV) technique to provide quantitative 3D information on micron-scale flows. The defocusing concept was implemented for use with fluorescence microscopy and a calibration procedure was outlined to establish the optical parameters needed to apply the standard DDPIV analysis. Sub-micron resolution has been verified and the measurement uncertainties have been fully determined. Time-resolved 3D flow mapping of a droplet internal circulation, caused by evaporation, was achieved with the spatial coordinates of particles inferred from their DDPIV images. Particle tracking velocimetry was used to derive the velocity field from the particle spatial field.

The microscopic defocusing technique (μDDPIV) introduced here provides a method to visualize and quantify 3D flows in a real-time manner. With an objective lens of higher magnification and smaller tracer particles, the system can be easily extended to sub-micron flow visualization.

The micron-scale imaging system can be adapted, in particular, to in vivo imaging of biological fluid systems. However, one limitation of the microscopic DDPIV technique, as put into practice in this work, is that it requires high intensity illumination because of the high f-number of the optical design. However, for in vivo biological fluid imaging, this intensity must be within reasonable limits to avoid damage to the biological system. Hence, future development in this direction will require the use of intensified, high-resolution and low-noise digital cameras.

Further study is also foreseen that will address the effect on the performance of μDDPIV of design parameters such as the numerical aperture of the objective lens and the size of the mask pinholes, as well as of external factors such as the size and density of particles.

References

Bown MR, MacInnes JM, Allen RWK, Zimmerman WBJ (2005) Three-component microfluidic velocity measurements using stereoscopic micro-PIV. In: Proceedings of 6th International Symposium on Particle Image Velocimetry (PIV'05)

Hove JR, Koster RW, Forouhar AS, Acevedo-Bolton G, Fraser SE, Gharib M (2003) Intracardiac fluid forces are an essential epigenetic factor for embryonic cardiogenesis. Nature 421:172–177

Inoué S, Spring KR (1997) Video Microscopy, 2nd edn. Plenum, New York

Jeon D, Pereira F, Gharib M (2003) Applications of defocusing DPIV to bubbly flow measurement. Part Part Syst Charact 20(3):193–198

Kajitani L, Dabiri D (2005) A full three-dimensional characterization of defocusing digital particle image velocimetry. Meas Sci Technol 16:790–804

Kang HK, Lee SJ, Lee CM, Kang IS (2004) Quantitative visualization of flow inside an evaporating droplet using the ray tracing method. Meas Sci Technol 15:1104–1112

Pereira F, Gharib M (2002) Defocusing digital particle image velocimetry and the three-dimensional characterization of two-phase flows. Meas Sci Technol 13(5):683–694

Pereira F, Gharib M, Dabiri D, Modarress D (2000) Defocusing digital particle image velocimetry: a 3-component 3-dimensional DPIV measurement technique. application to bubbly flows. Exp Fluids 29(7):S78–S84

Pereira F, Stüer H, Castaño-Graff E, Gharib M (2006) Two-frame 3D particle tracking. Meas Sci Technol 17:1680–1692

Prasad AK, Adrian RJ (1993) Stereoscopic particle image velocimetry applied to liquid flows. Exp Fluids 15:49–60

Pu Y, Song X, Meng H (2000) Off-axis holographic PIV for diagnosing particulate flows. Exp Fluids 29:S117–S128

Santiago JG, Wereley ST, Meinhart CD, Beebe DJ, Adrian RJ (1998) A particle image velocimetry system for microfluidics. Exp Fluids 25:316–319

Soloff SM, Adrian RJ, Liu ZC (1997) Distortion compensation for generalized stereoscopic particle image velocimetry. Meas Sci Technol 8:1441–1454

Suzuki H, Nakano M, Kasagi N, Ho CM (2003) Particle tracking velocimetry measurement of chaotic mixing in a micro mixer. In: Proceedings of International Symposium on Micro-Mechanical Engineering (ISMME2003), Tsuchiura, Japan

Willert CE, Gharib M (1992) Three-dimensional particle imaging with a single camera. Exp Fluids 12:353–358

Wu M, Roberts JW, Buckley M (2005) Three-dimensional fluorescent particle tracking at micron-scale using a single camera. Exp Fluids 38:461–465

Yoon SY, Kim KC (2006) 3D particle position and 3D velocity field measurement in a microvolume via the defocusing concept. Meas Sci Technol 17:2897–2905